Light-Scattering and TEM Analyses of Virtual Upper Critical Solution Temperature Behavior in PCL/SAN Blends

Petr Svoboda, Jörg Kressler, Tsuneo Chiba, and Takashi Inoue*

Department of Organic and Polymeric Materials, Tokyo Institute of Technology, Ookayama, Meguro-ku, Tokyo 152, Japan

Hans-Werner Kammer

Institut für Makromolekulare und Textilchemie, TU Dresden, Mommsenstrasse 4, D-O-8027 Dresden, Germany

Received July 7, 1993; Revised Manuscript Received November 12, 1993®

ABSTRACT: It has been known that blends of poly(ϵ-caprolactone) (PCL) and poly(styrene-*ran*-acrylonitrile) (SAN) show a miscibility window and, at the edges, lower critical solution temperature (LCST) behavior occurs. The presence of a virtual upper critical solution temperature (UCST) of PCL/SAN blends was found at lower temperatures as follows. Time-resolved light scattering under V_v and H_v optical alignments was used in order to distinguish two competitive processes—crystallization and liquid–liquid phase separation of blends quenched below the melting point. Three types of measurements were carried out in order to obtain the information: (1) kinetics of phase separation vs crystallization by using the invariant, (2) the most probable wavenumber of concentration fluctuation q_m having the highest growth rate, (3) the apparent diffusion coefficient. The positions of the virtual UCST obtained by different methods were in good agreement with each other. In total, the LCST's and UCST's form a closed miscibility area for PCL/SAN blends in the temperature–copolymer composition plane. This behavior is interpreted in terms of an equation-of-state theory. TEM micrographs were taken in order to confirm the difference in morphology between the blends quenched below and above the virtual UCST. The photographs showed the familiar lamellar crystal-amorphous structure for a system crystallized above the UCST and a morphology segregated to PCL-rich and SAN-rich phases for the same blend crystallized below the UCST.

Introduction

Poly(ϵ-caprolactone) (PCL) is miscible on a molecular level with poly(styrene-*ran*-acrylonitrile) (SAN) when the copolymer contains from 8 to 28 wt % acrylonitrile.[1] At the edges of the miscibility window, LCST (lower critical solution temperature) behavior has been observed, and in the center of the miscibility window, the blends are miscible above the melting temperature (T_m) of PCL (about 71 °C) until thermal decomposition. Below T_m, neat PCL lamellae are growing (crystallization), and between them, a homogeneous mixture of amorphous PCL and SAN should remain. The crystallization behavior of PCL is strongly influenced when amorphous SAN is present.[2] There is some evidence for a virtual liquid–liquid phase separation from a recent study of crystallization kinetics.[3] When the UCST (upper critical solution temperature) is located below T_m, it is conceivable that by a rapid temperature drop the region of liquid-phase instability could be reached where liquid–liquid demixing advances prior to crystallization.

In order to determine the UCST-type phase boundary of PCL/SAN blends, light scattering studies of the competitive processes, crystallization and liquid–liquid phase separation, are carried out. Samples are heated well above T_m and then crystallized isothermally at different crystallization temperatures. The virtual phase boundary below T_m is obtained by kinetic analysis of both liquid–liquid phase separation and crystallization. Furthermore, transmission electron microscopy (TEM) is applied to study the phase morphology of samples quenched to different temperatures. Finally, the phase behavior will be discussed in terms of an equation-of-state (EOS) theory.

* To whom correspondence should be addressed.
® Abstract published in *Advance ACS Abstracts*, February 1, 1994.

Experimental Section

The PCL was a commercial one of Union Carbide Corp. (PCL-700). The copolymers of styrene and acrylonitrile (SAN) were synthesized at 60 °C using ethylbenzene as a solvent and an AIBN concentration of 0.02 mol/L. The final conversion was less than 5%. The molecular weight data are given in Table 1. The blends were prepared by casting a 10 wt % solution of both polymers in 1,2-dichloroethane onto a cover glass. The solvent was evaporated at room temperature, and the samples were dried for 2 days in a vacuum oven. The thickness of the specimens was 20 ± 1 μm.

The specimens were annealed at 120 °C for 5 min on a hot stage. Then the specimens were rapidly quenched to the desired crystallization temperature (T_c) by putting them onto another hot stage set perpendicular to the laser beam (He–Ne laser of 632.8-nm wavelength). An analyzer was placed between the sample and photodiodes. Two optical geometries were used: (1) the H_v geometry in which the optical axis of the analyzer was set perpendicular to that of the polarizer and (2) the V_v geometry with a parallel set of the two axes. The V_v and H_v scattering data were obtained in separate runs. For one temperature, always the same sample was used. The angular distribution of scattered light intensity was detected by a one-dimensional photometer with a 46-photodiode array (HASC Co., Ltd.). The scattering profiles were measured at appropriate intervals and stored in a Forth Engine computer for further analysis.[21]

For the TEM analysis, ultrathin sections were microtomed from crystallized samples and stained with RuO_4. The TEM micrographs were obtained with a JEM 100CX microscope with an accelerator voltage of 100 kV.

Determination of Virtual UCST Behavior

The scattering of light caused by crystalline polymers arises in part from fluctuations in the average refractive index and in part from fluctuations in the orientation of anisotropic entities.[5] These contributions can be quantitatively separated by applying polarized light. The contribution from anisotropic fluctuations can be detected in a H_v configuration, while contributions of density

0024-9297/94/2227-1154$04.50/0

Table 1. Molecular Weight Data of All Polymers

polymer	$\bar{M}_w$, g/mol	$\bar{M}_w/\bar{M}_n$
PCL	40 400	2.61
SAN-12.4[a]	142 000	2.11
SAN-19.5	130 000	2.50
SAN-26.4	168 000	2.21

[a] Index means wt % of acrylonitrile in SAN.

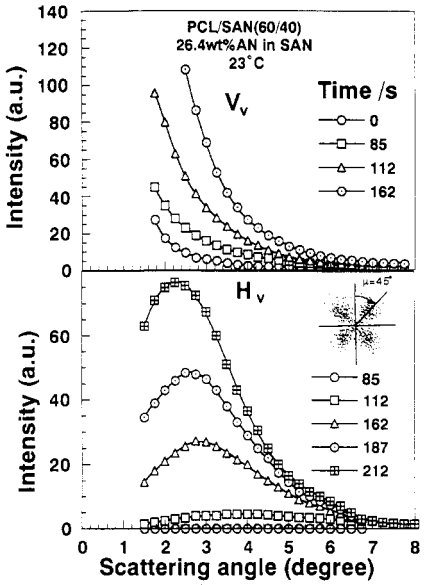

Figure 1. Change of V_v and H_v scattering profiles with time after quenching the PCL/SAN-26.4 (60/40) blend to 23 °C; H_v profiles are at azimutal angle $\mu = 45°$.

(refractive index) and orientation fluctuations are detected by a V_v configuration.[6] Time-resolved scattering profiles obtained for V_v and H_v optical alignments are shown in Figure 1. There is a significant change in the V_v profile from the start of the measurement (0 s) until 85 s, whereas the H_v profile remains at a zero level until 100 s and then a significant increase of the intensity can be seen. That means, the H_v profile does not change for a certain period of time, while the V_v scattering is increasing rapidly. It implies that density fluctuations caused by two isotropic phases precede the evolution of optical anisotropy. In other words, before crystallization starts, liquid–liquid phase separation occurs; i.e., the sample seems to be crystallized below the UCST in the two-phase region.

For the quantitative evaluation of kinetics of crystallization and liquid–liquid phase separation, it is convenient to use the invariant Q, i.e., the integrated scattering intensity[6]

$$Q = \int_0^\infty I(q)\, q^2\, dq \qquad (1)$$

where q is the scattering vector $q = (4\pi/\lambda)\sin(\theta/2)$, λ and θ being the wavelength and scattering angle, respectively, and $I(q)$ is the intensity of scattered light at q.

The time variations of the invariants Q_{H_v} and Q_{V_v} are plotted in Figure 2. The values of both invariants are increasing with time of annealing. Q_{H_v} starts to increase after a certain time lag when Q_{V_v} has already reached a relatively higher level. The rapid increase of Q_{V_v} and the slow increase of Q_{H_v} after the time lag may suggest that the liquid–liquid phase separation precedes and the crystallization follows. In other words, the crystallization temperature locates below the UCST and crystallization starts after the phase separation proceeds to a certain level.

Furthermore, one can discuss the location of the UCST from the relative increase of Q_{V_v} normalized by that of

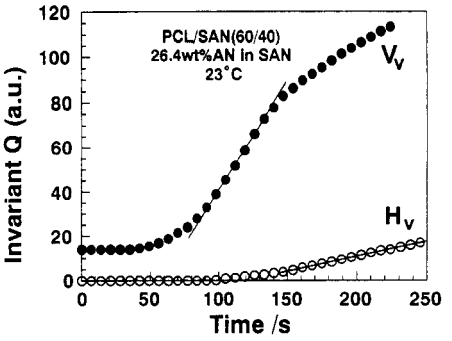

Figure 2. Time dependence of V_v and H_v invariants for PCL/SAN-26.4 (60/40).

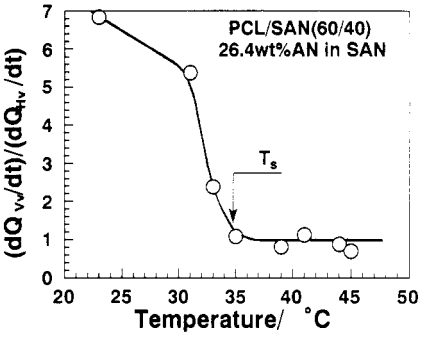

Figure 3. Temperature dependence of the relative value $(dQ_{V_v}/dt)/(dQ_{H_v}/dt)$.

Q_{H_v}. The initial slope of the time variation of Q_{H_v} (straight line in Figure 2), dQ_{H_v}/dt, is supposed to be a rate of crystallization[7] for systems without phase separation, while dQ_{V_v}/dt is composed of two rates below the UCST—(1) crystallization and (2) liquid-liquid phase separation. The ratio $(dQ_{V_v}/dt)/(dQ_{H_v}/dt)$ is a relative measure of the rate of the crystallization and phase separation. For the neat PCL, the ratio remains constant (about 1) for all measured temperatures. But a totally different situation arises after quenching the blend (Figure 3). A clear discontinuity appears. At lower temperatures, the ratio exhibits a relatively large value of about 7, and then a sharp decrease occurs to about 1 and remains constant at higher temperatures. Thus, the temperature at which the ratio deviates from 1 means the spinodal temperature. It implies that above the spinodal temperature (T_s) only crystallization takes place, while below T_s liquid-liquid phase separation proceeds, suggesting the UCST type of phase behavior.

For further analysis of the liquid-liquid phase separation, it should be mentioned that at the very early stage the contribution of crystallization to the overall V_v scattering is nearly zero (see Figures 1 and 2) so that one can discuss the details of the liquid-liquid phase separation by the initial time variation of I_{V_v} at a time window before the onset of crystallization. Below the UCST, the linear theory of spinodal decomposition[8] can be applied for data analysis. In the initial stage of phase separation, the intensity of scattered light (I) varies exponentially with time t.

$$I_{V_v}(q,t) \propto \exp[2R(q)t] \qquad (2)$$

where $R(q)$ is the growth rate of concentration fluctuations having the scattering vector q and is given by

$$R(q) = -Mq^2\left(\frac{\partial^2 f}{\partial c^2} + 2\kappa q^2\right) \qquad (3)$$

where M is the mobility, f is the free-energy density of the blend with composition c (volume fraction of one com-

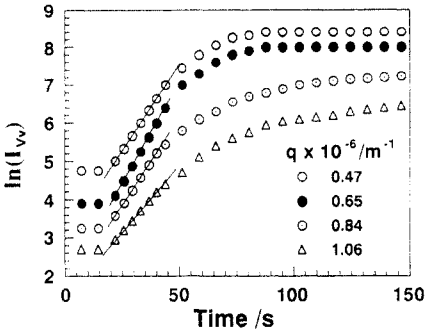

Figure 4. Time dependence of the scattered light intensity of different scattering vectors q after temperature drop to 25 °C for PCL/SAN-12.4 (60/40) blend.

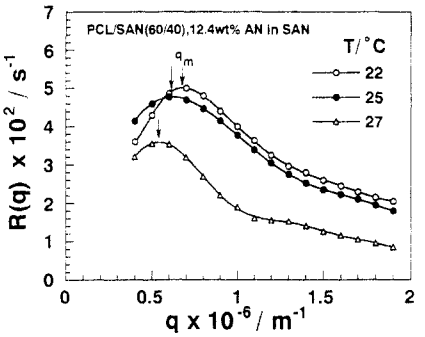

Figure 5. Dependence of $R(q)$ on q for different temperatures.

ponent), and κ is the gradient energy coefficient. One can estimate the growth rate $R(q)$ for the fluctuations from the initial slope of a ln I vs t plot (Figure 4) for different values of q. Figure 5 shows the $R(q)$ spectrum for different temperatures. For temperatures below the UCST, the curves exhibit a maximum at q_m. The position of the maximum changes with the distance from T_s. The dependence of q_m on the difference between the spinodal and annealing temperatures can be deduced easily. Equation 4 is obtained from eq 3 in the case that $[dR(q)/dq]$ is set to zero

$$q_m^2 = -(\partial^2 f/\partial c^2)/4\kappa \tag{4}$$

de Gennes theory for the spinodal decomposition of incompressible mixtures[9] leads to

$$\frac{\partial^2 f}{\partial c^2} = \frac{\chi - \chi_s}{\chi_s} \tag{5}$$

where χ is the Flory–Huggins interaction parameter and χ_s is the interaction parameter at the spinodal. Furthermore, it was shown that[10]

$$\frac{\chi - \chi_s}{\chi_s} \propto |T - T_s| \tag{6}$$

From eqs 4–6, it follows that

$$q_m^2 \propto |T - T_s| \tag{7}$$

It follows that at the spinodal ($T = T_s$)

$$\left(\frac{\partial^2 f}{\partial c^2}\right)_{T,p} = q_m^2 = 0 \tag{8}$$

Thus, the temperature dependence of q_m^2 can be used to obtain T_s as shown in Figure 6. When eqs 7 and 8 were

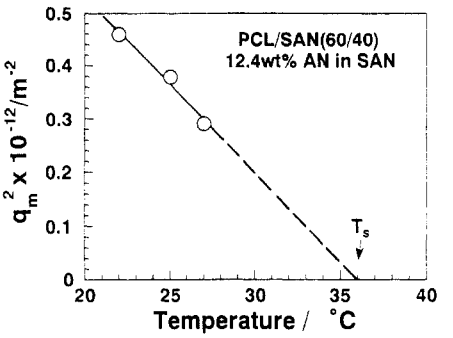

Figure 6. Temperature dependence of q_m^2 of a PCL/SAN-12.4 (60/40) blend.

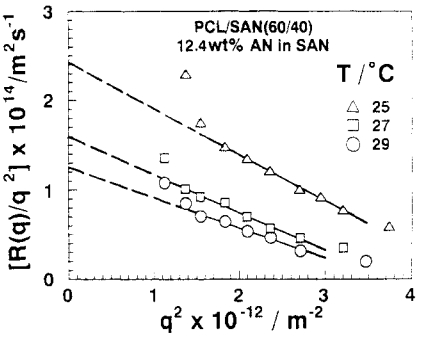

Figure 7. Plot $R(q)/q^2$ vs q^2 for different temperatures of a PCL/SAN-12.4 (60/40) blend.

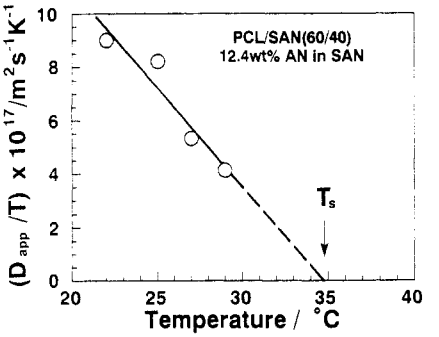

Figure 8. Temperature dependence of D_{app}/T for a PCL/SAN-12.4 (60/40) blend.

applied, T_s was taken as the intercept from the extrapolation of the straight line to $q_m^2 = 0$.

Furthermore, the spinodal temperature can be obtained from the temperature dependence of the apparent diffusion constant (D_{app}) which is defined by[10,11]

$$D_{app} = -M\left(\frac{\partial^2 f}{\partial c^2}\right) \tag{9}$$

By use of eqs 3 and 9, D_{app} can be obtained from $R(q)/q^2$ vs q^2 plots as the intercept of the $R(q)/q^2$ axis as shown in Figure 7. Since $M \propto T$, according to the Stokes–Einstein equation, and because of eqs 5 and 6, the temperature dependence of D_{app} in the vicinity of the spinodal is given by

$$D_{app} \propto T|T - T_s| \tag{10}$$

The spinodal temperature can be obtained from the D_{app}/T vs T plot as the intercept of the straight line with the temperature axes (Figure 8) because at the spinodal temperature D_{app} is 0.

The spinodal temperatures were obtained for a fixed blend ratio (PCL/SAN 60/40) and three different copolymer compositions by using three different methods as discussed before. All obtained values of T_s are plotted as

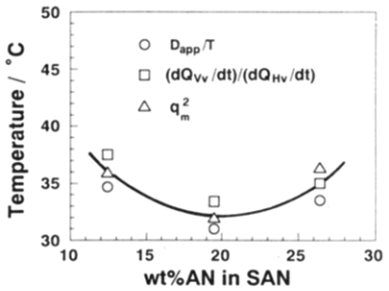

Figure 9. UCST border of PCL/SAN (60/40) blends.

a function of copolymer composition (Figure 9), creating a UCST border of PCL/SAN blends. It is reasonable that the curve has a minimum because according to thermodynamic calculations the miscibility window might be a "closed" area under some circumstances.[4]

TEM was applied in order to support the light-scattering methods of the determination of UCST behavior. Parts a and b of Figure 10 show TEM micrographs of a sample crystallized at 46 °C, above the virtual UCST. A TEM micrograph of the same sample quenched to 24 °C, below the UCST, can be seen at Figure 10c. The white regions are PCL rich, while the black regions are SAN rich, caused by staining of the phenyl ring by RuO_4. In parts a and b of Figure 10, it is possible to see the white lamellae of PCL very clearly and between them the amorphous region composed of a mixture of PCL and SAN is located. It implies the crystallization of the blend above the UCST from a homogeneous mixture. A completely different structure can be seen in Figure 10c. SAN-rich domains (dark regions of about 0.1 μm) can be clearly distinguished from the continuous PCL-rich phase. The white background should be the PCL-rich phase containing a large amount of amorphous and crystalline PCL. The lamellae of PCL cannot be detected because the amount of SAN may be too small in order to provide an effective staining contrast. This structure proposes an idea of crystallization after liquid-liquid phase separation reached a certain level; i.e., the sample was quenched below the UCST.

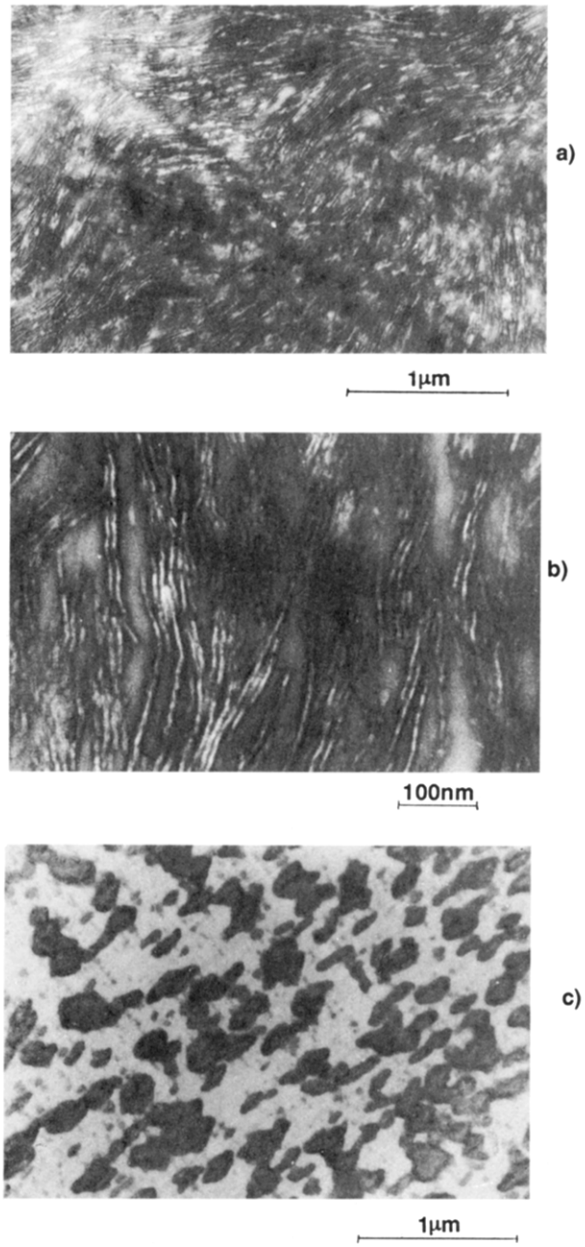

Figure 10. TEM micrographs of a PCL/SAN-12.4 (60/40) sample quenched to 46 °C (above UCST) with two different magnifications (a, b). The same sample quenched to 24 °C (below UCST) (c).

Thermodynamic Analysis

There has been an increasing number of reports about the simultaneous occurrence of a LCST as well as a UCST in blends of high molar mass polymers. One well-studied example is the blend system poly(methyl methacrylate)/poly(vinylidene fluoride).[12,7] So far, most of these systems with the simultaneous occurrence of the LCST and UCST contain at least one random copolymer. Some examples are blends of polybutadiene/poly(styrene-*ran*-butadiene),[13,14] SAN/poly(acrylonitrile-*ran*-butadiene),[15] and polystyrene/carboxylated poly(2,6-dimethyl-1,4-phenylene oxide).[16] This behavior will be discussed in terms of an equation-of-state theory proposed previously.[4] The starting point is the standard expression of Flory and Huggins for the Gibbs free energy of mixing per mole of lattice sites[17]

$$\frac{\Delta G}{RT} = \frac{\phi}{r_A}\ln\phi + \frac{1-\phi}{r_B}\ln(1-\phi) + X\phi(1-\phi) \qquad (11)$$

where r_i and ϕ denote the degree of polymerization of component i and the volume fraction, respectively. Here, we substitute, however, the interaction parameter of the original theory by a generalized free-energy parameter (X) which can be seen as a function of reduced temperature ($\tilde{T}$) and volume ($\tilde{V}$). This quantity may be expanded in powers of $1/\tilde{T}$ and $\tilde{V}$ around component A taken to be the reference substance. It results when higher than second-order derivatives are ignored[4]

$$X = \frac{\tilde{V}_A^{1/3}}{\tilde{V}_A^{1/3}-1}\left(2X_{AB} + 9\rho^2 - \frac{3}{4}\Gamma\rho + \frac{\frac{4}{3}-\tilde{V}_A^{1/3}}{\tilde{V}_A^{1/3}-1}\frac{9}{8}\rho^2\right) + \frac{\tilde{V}_A^{1/3}}{\frac{4}{3}-\tilde{V}_A^{1/3}}\frac{7}{8}\Gamma^2 \qquad (12)$$

Overall interaction and free-volume effects are represented by the parameters X_{AB} and Γ, respectively, while the parameter ρ accounts for the size effect. Moreover, $\tilde{V}_A$ is the reduced volume of component A (reference substance; $\tilde{V}_A \equiv V/V_A^*$, where the starred quantity symbolizes the reference parameter. The prefactors in the terms of eq 12 are positive definite and govern the temperature dependence of X. The quantities X_{AB}, Γ, and ρ can be expressed

Table 2. Reference Temperatures and Individual Parameters for the System PCL/SAN

polymer	T^*, K	r	$\chi_{i/j}$		δ_i		δ_i^r	
PCL	7200	354	CL/S	2.9×10^{-3}	S	0.153	S	0.036
PS	8300		CL/AN	0.0367	AN	0.271	AN	0.054
PAN	9150		S/AN	0.12				
SAN		1000						

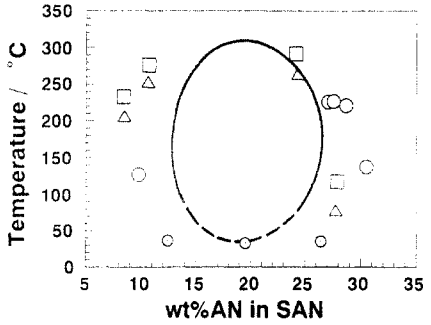

Figure 11. Miscibility map for the system PCL/SAN as a function of copolymer composition as calculated from eq 15 using the parameters of Table 2. (⊙) UCST reported in this paper, (□) LCST of PCL/SAN (30/70) blends taken from ref 1, (△) LCST of PCL/SAN (50/50) blends taken from ref 1, (○) LCST of PCL/SAN (30/70) blends taken from ref 18.

by individual segmental-based quantities for a blend comprising a random copolymer. It follows when A = PCL and B = SAN[4]

$$X_{AB} = \beta\chi_{CL/S} + (1-\beta)\chi_{CL/AN} - \beta(1-\beta)\chi_{S/AN}$$

$$\Gamma = \beta\delta_S + (1-\beta)\delta_{AN} - 2\beta(1-\beta)\chi_{S/AN}$$

$$\rho = \beta\delta_S^r + (1-\beta)\delta_{AN}^r \qquad (13)$$

where β is the mole fraction of styrene in SAN, $\chi_{i/j}$ represents the interaction parameter between segments of type i and j, and δ_i and δ_i^r stand for

$$\delta_i \equiv \frac{T_i^*}{T_A^*} - 1 \qquad \delta_i^r \equiv \frac{(V_i^*)^{1/3}}{(V_A^*)^{1/3}} - 1 \qquad (14)$$

where T^* is the respective reference temperature. By use of these equations, critical points as a function of copolymer composition are given by

$$X_{crit} - X = 0 \qquad (15)$$

where

$$X_{crit} = 1/2\left(\frac{1}{r_A^{1/2}} + \frac{1}{r_B^{1/2}}\right)^2 \qquad (16)$$

The reference temperatures (T^*) of the components and the parameter $\chi_{S/AN}$ have been submitted elsewhere.[18,19] Using the respective critical temperatures, one can estimate the remaining four unknown parameters $\chi_{CL/S}$, $\chi_{CL/AN}$, δ_S^r, and δ_{AN}^r from eq 15. All parameters involved in eq 13 are listed in Table 2. A miscibility map calculated according to eq 15 with the parameters of Table 2 is shown in Figure 11, where the virtual UCST's are distinguished by different markers from the LCST's. For clarification of Figure 11, it has to be mentioned that the LCST data do not necessarily represent the critical points, because they refer to mixtures of fixed but not necessarily critical compositions. So the real critical temperatures might be shifted to somewhat lower values. It should be noted that the LCST means a real equilibrium liquid-liquid phase separation. The situation becomes more complicated in the case of UCST behavior because a crystalline component below its equilibrium melting point is involved. But for kinetical reasons, it is possible that liquid-liquid phase separation precedes crystallization. Miscibility thus determined occurs inside the curve. As can be seen, the calculated miscibility region corresponds fairly to experimental data points. This miscibility map is determined by a complex interplay of the parameters X_{AB}, Γ, and ρ. However, one may say that the locations of virtual UCST and LCST are predominantly governed by the parameters ρ^2 and Γ^2, respectively. Owing to the vast value of parameter ρ (around 0.04), the UCST is shifted to rather high temperatures.

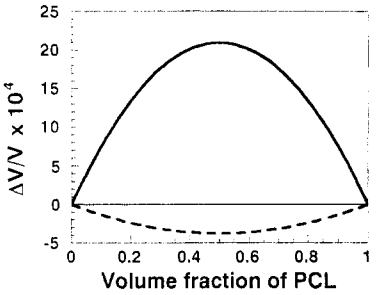

Figure 12. Volume of mixing for PCL/SAN-22 at 85 °C (solid curve) and at 260 °C (dashed curve).

It is worthwhile to estimate also the volumes of mixing. One can calculate the relative volumes of mixing, $\Delta V/V$, in the same approximation as the free-energy parameter (X) of eq 12. It follows[20] that

$$\frac{\Delta V}{V\phi(1-\phi)} = \frac{3}{4}\rho\left(\Gamma + \frac{11}{2}\rho\right) + \frac{\tilde{V}_A^{1/3} - 1}{\frac{4}{3} - \tilde{V}_A^{1/3}}\left(2X_{AB} - \frac{3}{4}\Gamma^2 + 9\rho^2 + \frac{9}{4}\rho\Gamma\right) - \frac{(\tilde{V}_A^{1/3} - 1)^2\left(\frac{14}{9} - \tilde{V}_A^{1/3}\right)}{\left(\frac{4}{3} - \tilde{V}_A^{1/3}\right)^3}\frac{3}{4}\Gamma^2 \qquad (17)$$

The results for two different temperatures are depicted in Figure 12 using the parameters of Table 2. A positive volume of mixing can be seen for miscible systems near the virtual UCST due to the large size effect, while the volume of mixing changes to negative values at sufficiently high temperatures.

Conclusion

Different light-scattering techniques were applied in order to determine quantitatively the position of the virtual UCST in PCL/SAN blends having different copolymer compositions. The existence of UCST behavior could also be confirmed by TEM. The occurrence of a "closed" miscibility window can be explained in terms of an EOS theory. Introduction of a parameter for different segment sizes may explain the change in the sign of the volume of mixing dependent on the temperature. Thus, the virtual UCST behavior is connected with a positive volume of mixing and the LCST behavior with a negative volume of mixing.

Acknowledgment. J.K. thanks the Japan Society for Promotion of Science for supporting his stay at TIT and the Humboldt Foundation for kind help. P.S. is grateful for a scholarship from the Ministry of Education, Science and Culture of Japan.

References and Notes

(1) Chiu, S. C.; Smith, T. G. *J. Appl. Polym. Sci.* **1984**, *29*, 1797.
(2) Kressler, J.; Kammer, H. W.; Silvestre, C.; DiPace, E.; Cimmino, S.; Martuscelli, E. *Polym. Networks Blends* **1991**, *1*, 225.
(3) Kressler, J.; Svoboda, P.; Inoue, T. *Polymer* **1993**, *34*, 3225.
(4) Kammer, H. W.; Inoue, T.; Ougizawa, T. *Polymer* **1989**, *30*, 888.
(5) Stein, R. S.; Erhard, P. F.; Clough, S. B.; Adams, G. *J. Appl. Phys.* **1966**, *37*, 3980.
(6) Koberstein, J.; Russell, T. P.; Stein, R. S. *J. Polym. Sci., Polym. Phys. Ed.* **1979**, *17*, 1719.
(7) Tomura, H.; Saito, H.; Inoue, T. *Macromolecules* **1992**, *25*, 1611.
(8) Cahn, J. W. *J. Chem. Phys.* **1965**, *42*, 93.
(9) De Gennes, P.-G. *J. Chem. Phys.* **1971**, *55*, 572.
(10) Hashimoto, T.; Kumaki, J.; Kawai, H. *Macromolecules* **1983**, *16*, 641.
(11) Inoue, T.; Ougizawa, T. *J. Macromol. Sci., Chem.* **1989**, *A26*, 147.
(12) Saito, H.; Fujita, Y.; Inoue, T. *Polym. J.* **1987**, *19*, 405.
(13) Ougizawa, T.; Inoue, T.; Kammer, H. W. *Macromolecules* **1985**, *18*, 2089.
(14) Bierlich, M.; Kressler, J.; Kammer, H. W. *Trends Polym. Sci. (India)* **1991**, *2*, 9.
(15) Ougizawa, T.; Inoue, T. *Polym. J.* **1986**, *18*, 521.
(16) Cong, G.; Huang, Y.; McKnight, W. J.; Karasz, F. E. *Macromolecules* **1986**, *19*, 2765.
(17) Flory, P. J. *Principles of Polymer Chemistry*; Cornell University Press: Ithaca, NY, 1953.
(18) Schulze, K.; Kressler, J.; Kammer, H. W. *Polymer* **1993**, *34*, 3704.
(19) Kammer, H. W.; Kressler, J.; Kressler, B.; Scheller, D.; Kroschwitz, H.; Schmidt-Naake, G. *Acta Polym.* **1989**, *40*, 75.
(20) Kammer, H. W. *Polymer* **1991**, *32*, 501.
(21) Okada, T.; Saito, H.; Inoue, T. *Macromolecules* **1992**, *25*, 1908.